geosciences

MDPI

Article

Coupling MRST-GEOPHIRES-X for Integrated Deep Geothermal Reservoir Simulation and Techno-Economic Assessment: A Proof of Concept

Diego Valdés Larraín [1], Ignasi Herms [2,*] and Enrique Gomez-Rivas [3]

[1] Màster d'Energies Renovables i Sostenibilitat Energètica, Facultat de Física, Universitat de Barcelona (UB), 08028 Barcelona, Spain; diegovaldeslarrain@gmail.com
[2] Àrea de Recursos Geològics, Institut Cartogràfic i Geològic de Catalunya (ICGC), 08038 Barcelona, Spain
[3] Departament de Mineralogia, Petrologia i Geologia Aplicada, Facultat de Ciències de la Terra, Universitat de Barcelona (UB), 08028 Barcelona, Spain; e.gomez-rivas@ub.edu
* Correspondence: ignasi.herms@icgc.cat

Abstract

The open-source evaluation of deep geothermal projects faces a structural gap between the physical analysis of subsurface reservoir conditions and the surface-level techno-economic assessment, traditionally bridged through inefficient manual coupling. To address this, an automated computational workflow controlled through a Python coupling interface was developed to integrate 3D thermo-hydraulic reservoir simulations in MRST (MATLAB Reservoir Simulation Toolbox) with the techno-economic tool GEOPHIRES-X. The architecture relies on synchronous batch-mode execution, incorporating a structural bypass of the native homogeneous subsurface models of GEOPHIRES-X. The resulting coupled workflow enables the automatic transfer of MRST reservoir simulation outputs, together with selected geometric parameters required for CAPEX calculations, to the GEOPHIRES-X techno-economic module. The workflow was tested with a case study of a deep geothermal doublet consisting of two J-type directional wells targeting a Jurassic reservoir in the Camp Basin, Catalonia (NE Spain), serving strictly as a methodological proof of concept to validate the tool's capabilities. The coupled analysis quantified the impact of reservoir heterogeneity and three-dimensional flow and heat transport that are not captured by standalone analytical tools: explicit 3D representations of vertical anisotropy and the buoyancy effects resulted in a 39.3% reduction in deliverable thermal power. Consequently, compared to the uncoupled baseline, the fully coupled model resulted in a 91.2% reduction in Net Present Value (NPV) and a 71.9% increase in the Levelized Cost of Heat (LCOH), reaching 0.1141 €/kWh$_{th}$. Additionally, an automated One-Factor-at-a-Time (OFAT) sensitivity analysis demonstrated that economic performance in the study area is more sensitive to surface operational variables than to the subsurface geological parameters considered. Finally, the proposed open-component coupling framework provides an auditable and reproducible interface between existing reservoir simulation and techno-economic tools, such as MRST and GEOPHIRES-X, enabling faster and more integrated geothermal assessments than separate model execution.

Keywords: coupling framework; deep geothermal energy; thermo-hydraulic simulation; techno-economic analysis; MRST; GEOPHIRES-X

Check for updates

Academic Editor: Gianluca Groppelli

Received: 29 October 2026
Revised: 15 November 2026
Accepted: 20 November 2026
Published: 24 November 2026

Copyright: © 2026 by the authors. Licensee MDPI, Basel, Switzerland. This article is an open access article distributed under the terms and conditions of the Creative Commons Attribution (CC BY) license.

1. Introduction

Geothermal energy is increasingly recognized as a critical renewable resource for industrial decarbonization through baseload power generation and direct heat use. However, in low-enthalpy systems (70–90 °C), where available exergy is constrained, commercial project feasibility strongly depends on minimizing distribution costs and accurately forecasting the long-term thermodynamic behavior of the reservoir. To be economically competitive against conventional fossil fuels, such projects require a rigorous initial techno-economic feasibility analysis.

A review of the current state of the research field reveals a structural disconnect between subsurface physics-based reservoir simulation models and Techno-economic assessment tools (TEA). Standard TEA tools, such as GEOPHIRES-X, are computationally efficient but typically rely on one-dimensional or semi-analytical reservoir models (e.g., Ref. [1]) assuming homogeneous, isotropic media. However, these simplified representations present major limitations when capturing 3D reservoir spatial heterogeneity, complex fluid and heat flow behavior, permeability anisotropy, and realistic well geometries. In contrast, open-source high-fidelity numerical simulators, such as the MATLAB Reservoir Simulation Toolbox (MRST) [2], can accurately model 3D geothermal grids and thermo-hydraulic behavior [3], resolving mass and energy conservation equations in heterogeneous porous media. This has been demonstrated, for example, in doublet and aquifer thermal energy storage systems [3], as well as in regional-scale geothermal potential screening workflows using structured multigrid simulations [4].

Bridging the gap between sophisticated 3D reservoir simulators and TEA approaches currently presents software and licensing barriers. Full thermo–hydraulic–economic workflows often rely on commercial or closed-source platforms (such as TOUGH2/TOUGH3 or CMG coupled with external cost spreadsheets [5]), limiting reproducibility and widespread academic or early-stage exploratory use. While there are advanced open-source subsurface codes (e.g., OpenGeoSys, PFLOTRAN, DuMuX), they generally lack integrated economic assessment modules. By contrast, specialized open-source TEA tools, such as GEOPHIRES-X, provide comprehensive surface facility and economic costing modules but lack native 3D distributed-parameter reservoir simulation capabilities. This makes the modular, open-source thermo–hydraulic–economic framework of MRST an ideal candidate for integration with TEA platforms. (Note: While GEOPHIRES-X and the core MRST modules are fully open-component, the execution of MRST relies on the proprietary MATLAB environment, meaning the proposed architecture operates as an open-component coupling framework built across a commercial numerical computing platform).

To overcome this limitation, this study presents a new automated computational workflow controlled via Python (3.15) that couples the 3D thermo-hydraulic reservoir simulations in MRST with the techno-economic assessment framework of GEOPHIRES-X. The workflow algorithmically overrides the native analytical subsurface estimations of GEOPHIRES-X by directly providing dynamically calculated thermal vectors and geometrically corrected capital expenditure (CAPEX) parameters derived from high-resolution MRST simulations.

It is important to emphasize that the primary objective of this manuscript is to present and validate the open-component coupling methodology itself. The proposed workflow is demonstrated using a case study considering a scenario of a hypothetical J-type directional doublet deployed in the highly transmissive karstified Jurassic dolostone reservoir located in the Camp Basin (Catalunya, NE Spain). This scenario is evaluated strictly as a functional proof of concept rather than an exhaustive regional resource assessment. The main findings demonstrate that uncoupled analytical models may provide an overly optimistic assessment of project viability, potentially overestimating profitability and underestimating the

levelized cost of heat (LCOH). By explicitly capturing 3D reservoir-scale physical and geological constraints, this coupled techno-economic framework helps correct biased financial projections and mitigate capital allocation risks in complex geothermal projects.

2. State of the Art and Theoretical Framework

2.1. Low-to-Medium Enthalpy Geothermal Systems

Low- to medium-enthalpy geothermal systems, characterized by temperatures below 150 °C, are primarily used for direct industrial heat or district heating, rather than for electricity generation [6]. The inherent thermodynamic challenge of these systems is their low exergy; the extracted fluid contains substantial thermal energy but a low capacity to perform useful work. Consequently, economic viability depends on minimizing distribution distances and integrating high-temperature heat pumps (HTHPs) to amplify the heat vector to meet specific industrial process demands. Exploitation typically relies on a doublet configuration (a production well and an injection well) that maintains the system's hydrostatic pressure and ensures resource sustainability. However, this geometry introduces the risk of premature thermal breakthrough, requiring precise spatial planning based on the petrophysical heterogeneity of the target aquifer.

2.2. Evolution of Geothermal Reservoir Simulation

Numerical simulation of geothermal reservoirs requires the coupled solution of mass and energy conservation equations in porous media, incorporating the dynamic properties of fluids and geological anisotropy. Historically, the industry standard has relied on tools such as the TOUGH2 Geothermal Reservoir Simulator to handle non-isothermal multiphase flows [7]. However, in recent years, the MATLAB Reservoir Simulation Toolbox (MRST) has consolidated its position as a leading, widely used open-source research framework. Recent studies have extensively validated the MRST geothermal module; for instance, Memon and Makauskas [8] utilized the framework to precisely track thermal front dynamics over time, while Nan et al. [9] and Shi et al. [10] coupled MRST with embedded discrete fracture models (EDFM) to rigorously simulate complex hydrothermal processes and heat transfer in fractured geothermal reservoirs. Moreover, advanced well stimulation techniques require a deep understanding of how damage evolves at the microscale. For instance, recent studies utilizing X-ray computed tomography (CT) and texture analyses via the Gray-Level Co-occurrence Matrix (GLCM) have demonstrated that cyclic thermal shocks using liquid nitrogen significantly increase both porosity and the connectivity of the fracture network in high-temperature crystalline rocks, such as granite [11,12]. However, in naturally transmissive carbonate sedimentary formations, like the one in our proof-of-concept study, reservoir simulation relies primarily on capturing pre-existing permeability architectures, rather than on artificially induced micro-damage networks.

Unlike simpler analytical models, MRST employs finite-volume methods that natively support 3D petrophysical heterogeneity. This capability is not merely an optional refinement but a physical necessity. In addition to this, an accurate characterization of temperature-dependent thermal conductivity and coupled heat transfer mechanisms is essential for developing a reliable geothermal model of the subsurface [13]. Recent literature highlights that capturing scales of heterogeneity and sedimentary architecture, as well as employing adequate grid resolution, is critical to accurately predicting fluid and heat flow [14]. Furthermore, studies such as those by Jia et al. [15] and Gao et al. [16] demonstrate how flow distribution is fundamentally dictated by pore sizes and complex fracture networks in highly heterogeneous carbonate reservoirs. Consequently, attempting to model highly transmissive, structurally anisotropic formations, such as the karstified Jurassic dolostone

reservoir in the Camp Basin, using isotropic assumptions, inevitably compromises the physical validity of the extracted thermal vectors.

2.3. GEOPHIRES-X and the Existing TOUGH2 Coupling: Limitations and the TOUGH3 Gap

The open-source GEOPHIRES techno-economic evaluation tool, designed for the integrated technical and economic assessment of geothermal projects, has evolved from its initial implementation (v1.0) through GEOPHIRES-2 described by [5] to the currently maintained GEOPHIRES-X platform [17]. GEOPHIRES-X combines reservoir, wellbore, and surface-plant technical models with capital (CAPEX) and operational (OPEX) cost correlations to estimate the levelized cost of energy (LCOE), net present value (NPV), and the lifetime thermal/electrical output of a geothermal project, supporting multiple end-use configurations (direct-use heat, electricity, and cogeneration).

By default, the tool employs simplified analytical models that assume homogeneous and isotropic rock masses to characterize reservoir behavior, coupled with a set of standardized economic models to perform the techno-economic calculations. For more advanced reservoir-modeling coupling possibilities, GEOPHIRES-X already permits substituting these analytical models with a numerical simulation via an existing coupling to the proprietary, license-based reservoir simulator TOUGH2. However, this integration presents notable limitations: it operates through a single-pass, unidirectional subprocess call to a locally installed executable, and relies on a comparatively rigid grid-construction routine that constrains the representation of three-dimensional geological bodies and their heterogeneities, such as fractures. Furthermore, this coupling remains tied specifically to TOUGH2's legacy output format; its successor, TOUGH3 [18] which consolidates the serial and massively parallel (TOUGH2-MP) codebases and is likewise distributed under a paid license from the Lawrence Berkeley National Laboratory (LBNL), is not natively supported, and integrating it requires manual source-code modifications to GEOPHIRES-X's reservoir-parsing routines.

2.4. The Coupling Gap in Techno-Economic Assessment

Proving the thermodynamic feasibility of a geothermal doublet is insufficient without demonstrating its financial viability through indicators such as Net Present Value (NPV), Levelized Cost of Heat (LCOH), and Internal Rate of Return (IRR). Open-source techno-economic tools, particularly GEOPHIRES-X, are widely used to estimate these indicators by calculating capital expenditures (CAPEX), such as drilling costs, and operational expenditures (OPEX), including pumping requirements. However, while GEOPHIRES-X offers several reservoir modelling options, its simplified analytical approaches may not adequately capture the spatial heterogeneity and transient thermo-hydraulic behavior of complex geological reservoirs.

Previous research has demonstrated significant advances in coupling numerical reservoir models with external tools. In particular, GEOPHIRES supports coupling with TOUGH2, enabling the integration of numerical reservoir simulation results into techno-economic assessments [5]. Furthermore, MRST has been coupled with external solvers to address complex multiphysics problems, including hydro-mechanical coupling in fractured rocks [19,20], peridynamics for hydraulic fracturing simulation [21], and coupled numerical models for assessing caprock geochemical integrity [22]. Other approaches have also integrated physics-based reservoir representations with surface infrastructure optimization frameworks [23].

Building upon the established capabilities of TOUGH2–GEOPHIRES coupling [5], the key methodological contribution of this study is the development of an automated coupling framework integrating two open-source tools, MRST and GEOPHIRES-X. Rather than seeking to improve upon the numerical capabilities of existing TOUGH2-based approaches,

the proposed methodology provides an accessible, transparent, and extensible alternative that avoids dependence on restrictively licensed reservoir simulation software. Although MRST is primarily developed for MATLAB, it also supports GNU Octave, a free and open-source alternative [2], further enhancing its accessibility and potential reproducibility. The proposed framework enables the automated integration of heterogeneous 3D thermo-hydraulic reservoir simulations into project-level techno-economic assessments, facilitating systematic parametric sensitivity analyses. Its scientific contribution is demonstrated by quantifying how geological heterogeneity and transient reservoir behavior influence thermal power production and economic indicators, particularly NPV and LCOH, compared with simplified analytical reservoir modelling approaches.

3. Materials and Methods

To bridge the gap in open-source geothermal assessment between physical reservoir characterization and techno-economic modeling tools, this work develops and implements an automated computational workflow coupling 3D reservoir simulation with techno-economic analysis. The methodology is structured around three main components: first, the characterization of the 3D thermo-hydraulic numerical model and the techno-economic engine; second, the design and implementation of the Python-based coupling architecture and the necessary mathematical data transformations; and finally, the parametric configuration of the specific case study.

3.1. Three-Dimensional Thermo-Hydraulic Modeling (MRST)

In this study, fluid flow and heat transport at the 3D reservoir scale are simulated using the open-source MATLAB Reservoir Simulation Toolbox (MRST) version *MRST 2025b*, specifically its Geothermal module [24] using MATLAB vR2025b. MRST supports a range of 3D structural and geological grid representations, including voxel-based, Cartesian, corner-point, and unstructured polyhedral grids, for subsurface flow and transport simulations. Here, a 3D voxet geological grid model is imported into the simulation framework, and lithological information is decoded using binary bitmasks to identify and isolate the target reservoir units. It should be noted that the petrophysical heterogeneity in the model is deterministically mapped from the discrete lithological facies of the ICGC 3D voxet, rather than being generated via continuous stochastic random fields. Consequently, probabilistic spatial correlation lengths are not applicable within this deterministic framework.

The governing equation used for energy conservation in the coupled fluid-rock system is defined as:

$$\frac{\partial}{\partial t}\left[\phi\rho c_p T + (1-\phi)\rho_r c_{p,r} T\right] + \nabla\cdot\left(\rho c_p \boldsymbol{u} T\right) = \nabla\cdot\left(\lambda_{ef}\nabla T\right) + q_e \quad (1)$$

where ϕ is the porosity, ρ and ρ_r are the fluid and rock densities, c_p and $c_{p,r}$ represent the specific heat capacities, λ_{ef} is the effective thermal conductivity, and q_e is the energy source term. On the other hand, mass conservation is governed by the continuity equation coupled with Darcy's law:

$$\frac{\partial(\phi\rho)}{\partial t} + \nabla\cdot(\rho\boldsymbol{u}) = q_m \quad (2)$$

$$\boldsymbol{u} = \frac{-\kappa}{\mu}(\nabla p - \rho g \nabla z) \quad (3)$$

where u is the Darcy velocity, κ is the permeability tensor, μ is the dynamic viscosity, and q_m represents the well mass source terms.

Furthermore, the numerical resolution also discretizes the 3D grid telescopically, thereby maximizing cell resolution strictly around the wellbores while applying boundary conditions at the edges. An important physical constraint integrated into the model is the

presence of a halocline, whereby salinity increases markedly with depth, increasing the non-linearity of the system.

To ensure transparency and full reproducibility of the subsurface physical model, the numerical configuration implemented in MRST is parameterized based on the ICGC's 3D geological and thermal models [25]. The simulation incorporates a 3D "voxet" style geological model, discretized using a telescopic grid centered on the area of interest (AOI). Fluid properties account for a brine salinity (total dissolved solids, TDS) of 22,676 mg/L (22.676 g/kg), with a fluid density of $\rho = 1016$ kg/m^3 and a dynamic viscosity defined as a function of temperature and salinity ($\mu = 0.83 \times 10^{-3}$ Pa · s at 30 °C). Furthermore, hydrogeological boundary conditions are established by imposing fixed pressure and temperature values at the lateral boundaries of the computational grid. The well configuration includes a drilling radius of $r = 0.15$ m (an 11.8-inch completion diameter), a constant mass production rate of 50.8 kg/s ($\sim$ 50 L/s), and a skin factor of $s = 2.0$. The simulation covers a 30-year operational horizon, discretized into 128 adaptive time steps. As highlighted throughout this study, this geological and operational configuration serves as a functional proof of concept designed to demonstrate the capabilities of the proposed open-component coupling framework; it is not intended as an exhaustive assessment of regional-scale resources. The fluid properties explicitly account for the input brine salinity, which modulates fluid density and dynamic viscosity as a function of temperature within MRST.

Non-linearities are resolved iteratively via the Newton–Raphson method, while the resulting linear systems are solved using the Generalized Minimal Residual method (GMRES) [26]. The complete physical simulation workflow, logically structured into inputs, processing, and outputs, is detailed in Figure 1.

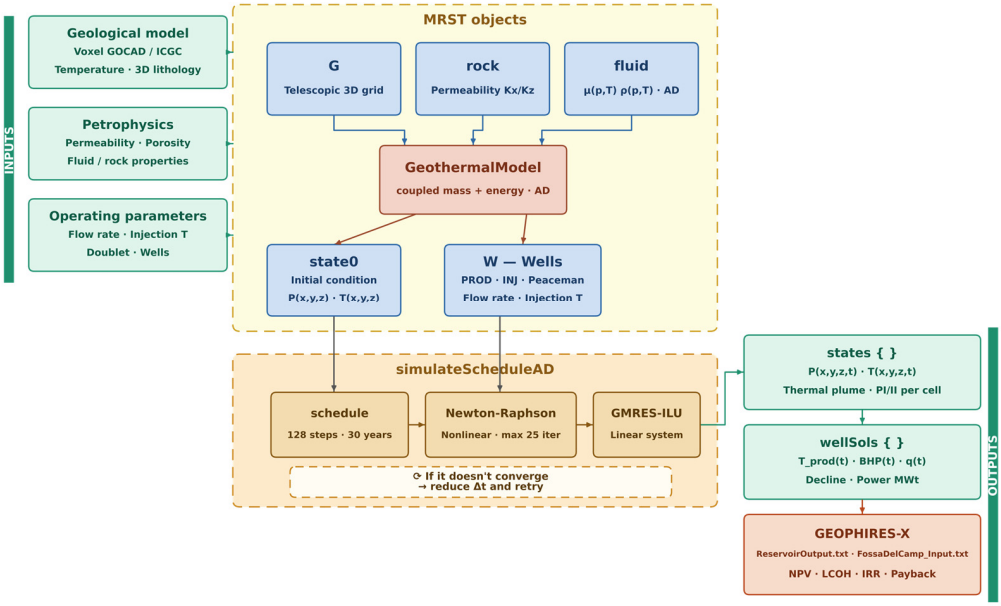

Figure 1. Detailed flowchart of the physical subsurface simulation performed by MRST.

3.2. Techno-Economic Engine and Algorithmic Bypass (GEOPHIRES-X)

GEOPHIRES-X [17] is structurally designed to carry out analytical subsurface evaluations that assume homogeneous and isotropic media. Specifically, GEOPHIRES-X offers nine distinct options for reservoir modeling. Although its default internal configurations are based on simplified analytical models that assume uniform and isotropic subsurface conditions, this workflow specifically employs "Reservoir Model Option 5", which allows the system to bypass its internal analytical calculations by directly incorporating externally

computed thermal vectors. The core innovation of this workflow is the algorithmic bypass of these native functions to enforce the assimilation of numerical results.

Upon execution, the Python coupling interface overrides the standard evaluation and injects the serialized $T(t)$ array directly into the GEOPHIRES-X reservoir submodule. This bypass forces downstream modules to operate strictly under the high-fidelity physical constraints derived from MRST:

- **Wellbore Thermodynamics**: The wellbore module utilizes the injected temperature curve imported directly from the MRST simulation to calculate heat losses during fluid ascent via the Ramey analytical model [4,17] and computes the required pumping power based on the stabilized productivity and injectivity (PI/II) indices imported from MRST.
- **Surface Plant Decoupling**: The surface plant module is dimensioned considering the integration of a high-temperature heat pump (HTHP). Crucially, it isolates the compressor's electrical consumption ($W_{elec} = Q_{out}/COP$) strictly as an Operational Expenditure (OPEX). This physical decoupling prevents common accounting artifacts in analytical models, where an increase in thermodynamic efficiency (COP) counterintuitively reduces the calculated net thermal revenue.
- **Financial Consolidation**: The economic module integrates the CAPEX and its geometric multiplier f_{CAPEX}, and aggregates the annual OPEX over the project's lifetime. It then processes the discounted cash flows to calculate the Net Present Value (NPV) and Levelized Cost of Heat (LCOH). All raw financial outputs native to GEOPHIRES-X (calculated in USD) were converted to Euros (EUR) using the European Central Bank average monthly exchange rate for May 2026 (1.00 EUR = 1.16 USD) [27] to reflect the European context of the case study. This exchange rate functions as a constant linear scalar applied to the final outputs, ensuring that all relative variations and sensitivity rankings remain mathematically unaffected by the currency conversion. Figure 2 illustrates the sequential execution of these modified submodules, demonstrating how external data dictates the economic evaluation.

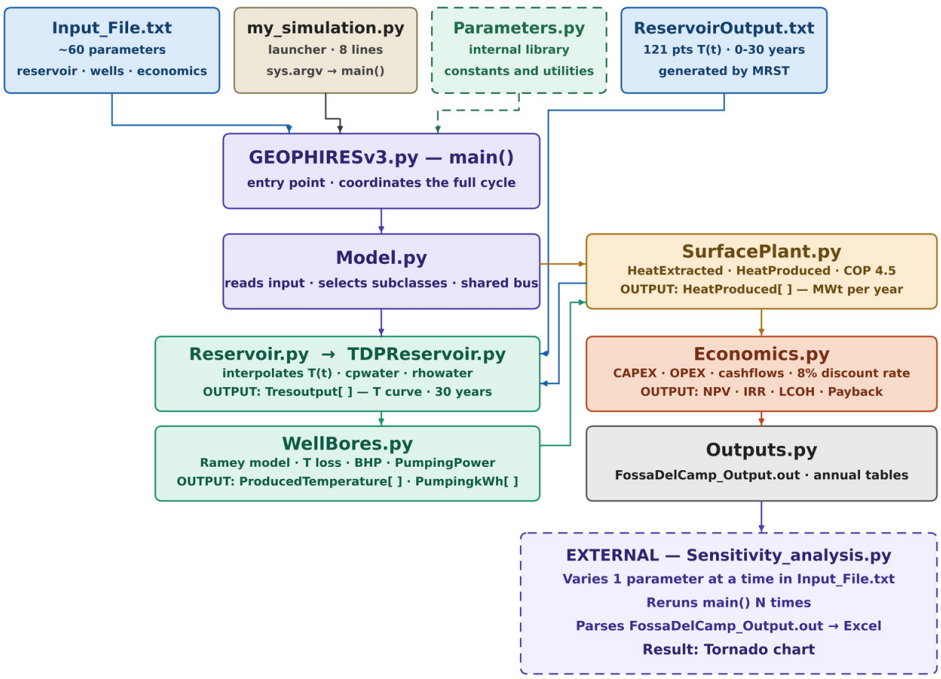

Figure 2. Flowchart of the Python-based techno-economic simulation architecture within GEOPHIRES-X.

3.3. System Architecture and Interoperability Strategy

To address the structural interoperability challenge between MATLAB (physical simulation) and Python (financial evaluation), this study implements a loose-coupling strategy orchestrated by a Python controller. This architecture isolates numerical modeling from economic evaluation, ensuring each iteration remains independent, auditable, and reproducible without modifying core source codes, and operates through a highly structured sequence of synchronous system calls and on-disk data serialization (Figure 3):

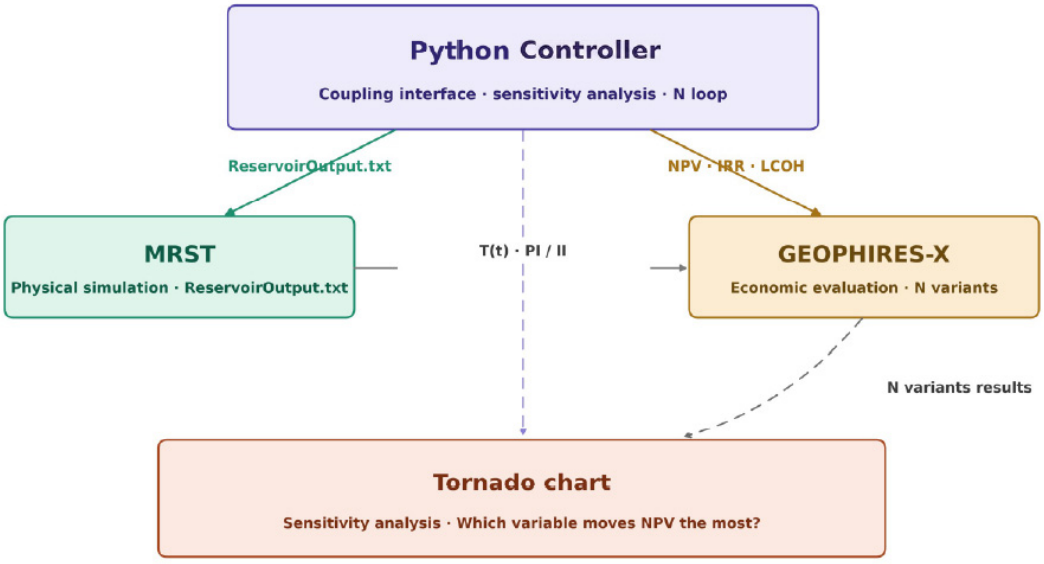

Figure 3. Configuration of the Python automation framework and loose-coupling strategy.

1. **Parametric Serialization**: The Python coupling interface initiates the sequence by dynamically generating an `mrst_params.json` file. This file contains the geometric, operational, and petrophysical variables specific to the current iteration, as well as those intended for analysis, allowing the workflow to modify the physical model externally.
2. **Execution and Concurrency Management**: Python launches the MATLAB environment in batch mode via a `subprocess` routine. Running in batch mode is critical, as it disables graphical rendering, preventing memory saturation during large-scale sensitivity analyses. To protect the workflow from divergent numerical iterations, the controller enforces a strict 900-s timeout protocol.
3. **Internal Interception**: A dedicated MATLAB wrapper script (`wrapper_mrst.m`) intercepts the JSON data upon initialization. This wrapper structures the execution within a *try*/*catch* block, ensuring that if a specific parametric combination fails to converge, the simulation is safely aborted, the error is logged, and the coupling interface seamlessly proceeds to the next iteration.

3.4. Interface Data Translation and Geometric Corrections

A direct transfer of raw output data from the physical simulator to the financial engine is unfeasible due to inherent differences stemming from both their native computational languages and the way they discretize time and space. Consequently, MRST is programmed to perform three critical intermediate mathematical transformations before exporting the data:

First, to address the temporal mismatch between MRST's adaptive time-stepping and the fixed-period cash flow requirements of GEOPHIRES-X, the physical simulator extracts and interpolates the continuous production temperature curve $T(t)$ into a regularized vector of 121 equidistant temporal points over the 30-year horizon. This temporal discretization is adopted to provide the time-series input required by GEOPHIRES-X and does not

constitute an independent verification of the numerical convergence of the underlying reservoir simulation.

Second, GEOPHIRES-X requires constant hydraulic resistances to estimate long-term pumping power. To reconcile this with the dynamic nature of the model, MRST analyzes the bottom-hole pressure (BHP) curves and, based on this, calculates stabilized and time-averaged Productivity (PI) and Injectivity (II) indices.

Third, analytical economic tools underestimate drilling-related Capital Expenditures (CAPEX) for directional wells by relying on True Vertical Depth (TVD) correlations. To correct this, MRST extracts the actual Measured Depth (MD) of the simulated wellbores from its 3D geometric grid, subsequently applying a polynomial cost correlation ($C_{well} = c_2 \cdot MD^2 + c_1 \cdot MD + c_0$) to both the TVD and the MD. The ratio between these costs generates a Well Drilling Adjustment Factor (f_{CAPEX}), defined formally as:

$$f_{CAPEX} = \frac{C_{PROD}(MD) + C_{INJ}(MD)}{C_{base}(TVD)} \quad (4)$$

where the polynomial coefficients for large-diameter deviated wells are established as $c_2 = 0.2173$, $c_1 = 1362.93$, and $c_0 = 301,066.16$. These values correspond to the baseline empirical cost correlations natively implemented in the Economics.py module of the GEOPHIRES-X source code [17].

To account for the geometric deviation of J-type wells, the cost evaluation compares the true vertical depth (TVD) against the measured depth (MD). Table 1 details the cost comparison between the vertical baseline and J-type directional wells, based on a geometric adjustment factor $f_{\mathrm{CAPEX}} = 2.652$ (evaluated using the May 2026 exchange rate of 1.00 EUR = 1.16 USD [27]).

Table 1. Geometric and drilling cost comparison between vertical reference wells and the simulated J-type directional doublet. (Note: The f_{CAPEX} multiplier is derived from the ratio of the total deviated cost to the vertical baseline doublet (20.50/7.73 = 2.652).

Well Configuration	Trajectory Type	Depth (TVD/MD) [m]	Estimated Drilling Cost [MEUR]
Vertical Reference (Single Well)	Vertical	2257/2257	~3.86
Vertical Baseline Doublet (x2)	Vertical	2257 (x2)	~7.73
J-Type Doublet (Producer)	Deviated	2257/4803	~10.22
J-Type Doublet (Injector)	Deviated	2257/4820	~10.28
Deviated Doublet Total	Deviated	-	~20.50

3.5. Example Case Study—The Camp Basin

The workflow was applied to the Camp Basin case study (Catalonia, NE Spain) (Figure 4), a Neogene basin located within the Catalan Coastal Ranges. The basin comprises Paleogene and Neogene sediments, deep Mesozoic aquifers, and a fractured Paleozoic basement composed mainly of granitoids. The specific geothermal target area is in the Mas del Batlle industrial zone, west of the urban center of the city of Reus (Figure 5, pink circle inside red rectangle).

A regional-scale 3D geological and thermal model with relatively coarse spatial resolution of the basin is available through the ICGC Geoíndex 3D Geological Resources Viewer [25]. The geological model was built in 3DGeomodeller® from the available geological information and refined through geophysical inversion of gravity and magnetic data. This geological framework was subsequently used to develop a preliminary 3D conductive thermal model of the whole Camp basin [25].

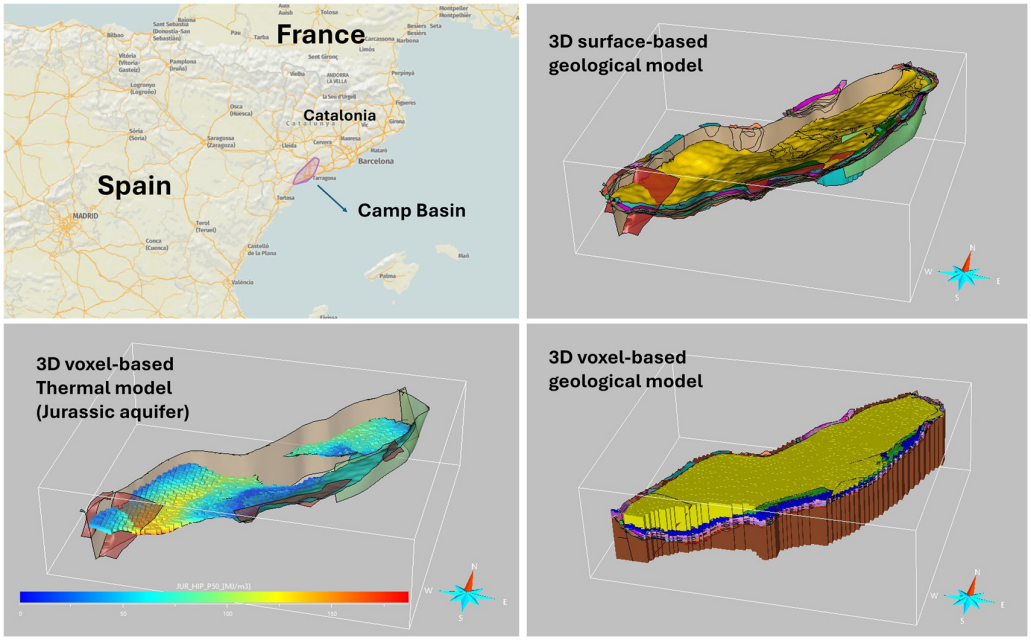

Figure 4. Situation of the study area—Camp Basin, in NE Spain; 3D regional-scale geological model: Surfaces, Voxels, Thermal model (adapted from [25]).

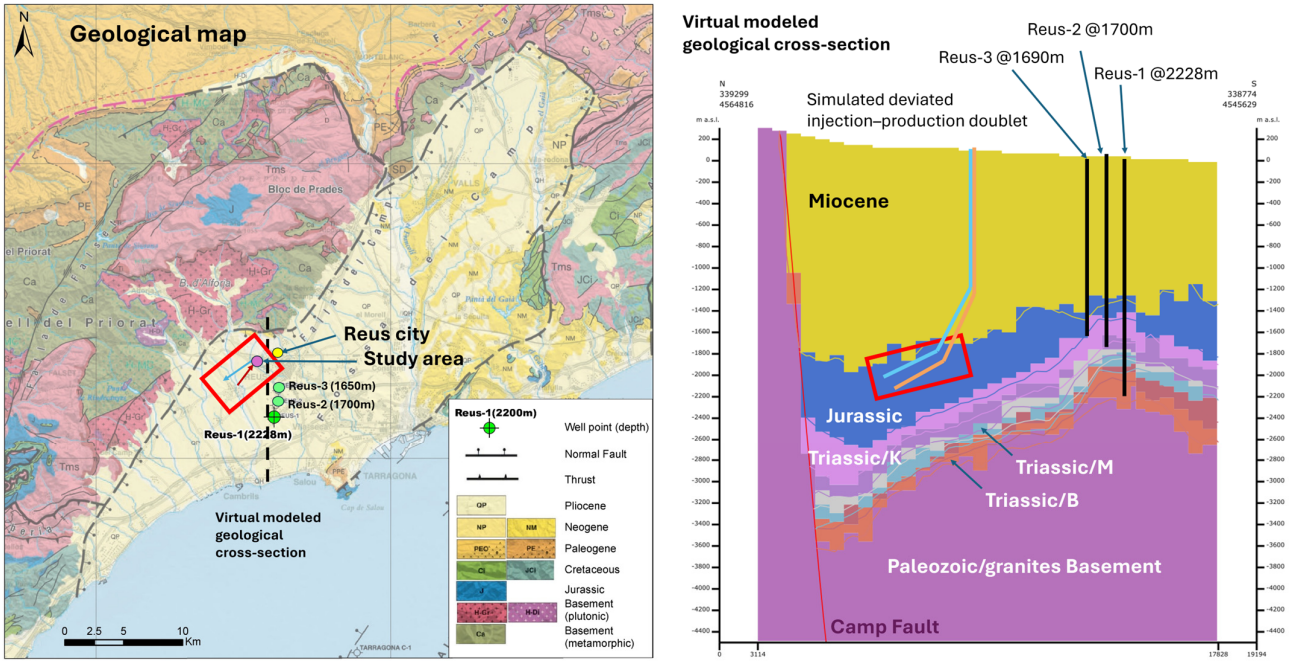

Figure 5. Geological map of the Camp Basin and virtual geological cross-section derived from the regional-scale 3D geological model, showing the Miocene deposits filling the basin, the underlying Mesozoic succession (Jurassic, Triassic (K)euper, (M)uschelkalk, and (B)untsandstein), the Paleozoic Basement and indication of the SW-NE Camp Fault. The cross-section also shows the location of the Reus-1, Reus-2, and Reus-3 deep wells, together with the deviated injection–production doublet implemented in the 3D MRST reservoir simulation.

The regional-scale 3D model shows a progressive deepening of the Mesozoic succession toward the northwest and the Camp Fault. Beneath the selected target area, the Jurassic carbonate aquifer is interpreted to occur at depths of approximately 1850–2450 m. These values should be regarded as approximate because no deep boreholes are available in this

part of the basin and the relatively coarse spatial resolution of the regional model introduces additional uncertainty at the local scale. The regional thermal model indicates a geothermal gradient of 30.31 °C/km, consistent with the available temperature measurements from the Reus-1, Reus-2, and Reus-3 wells. Assuming a mean surface temperature of 15 °C, the uppermost ~150 m of the reservoir, considered the main transmissive interval and located approximately between 1850 and 2000 m depth, would correspond to temperatures of approximately 71–76 °C. Temperatures increase with depth within the Jurassic succession, with the regional 3D thermal model predicting maximum reservoir temperatures of up to ~85 °C in the deepest sections of the aquifer.

The closest direct subsurface information comes from the Reus-1, Reus-2, and Reus-3 wells, located approximately 4–4.5 km southeast of the target area. These are the only historical deep wells in the basin that reach the Mesozoic aquifers and intersect the Jurassic succession. Reus-1, drilled by APEX–CAMPSA–SHELL in 1976, reached a total depth of 2228 m [28] while Reus-2 and Reus-3 reached 1700 m [29] and 1690 m [30], respectively.

The Jurassic formation is approximately 240–260 m thick in Reus-1 and Reus-2, reaching approximately 261 m in Reus-1 and 241 m in Reus-2, where it extends from approximately 1388 to 1629 m. In contrast, Reus-3 encountered only about 38 m of Jurassic rocks, as the well is located near the fault-bounded margin of a structural paleohigh previously investigated during the years 1996–2001 for geological gas storage [31]. Toward the northwest, however, the regional 3D model indicates renewed deepening and thickening of the Jurassic succession beneath the target area [25]. The upper part of the Jurassic succession consists mainly of fractured, karstified, and locally brecciated dolomitic carbonates and represents the main aquifer interval. Based on the available geological and hydraulic evidence, the uppermost ~150 m were interpreted as the principal transmissive interval [28].

Production tests conducted in Reus-2 show substantial vertical variations in the hydraulic properties of the Jurassic reservoir. A test covering the main dolomitic interval (1389–1589 m) yielded an estimated permeability of 2930 mD, whereas the uppermost tested interval (1389–1430 m) yielded an estimated permeability of 13,200 mD [29]. These results support the interpretation of the upper karstified dolostone as the most transmissive part of the Jurassic aquifer. To construct a stable numerical model for the entire 150 m transmissive bulk reservoir, the 2930 mD value was deemed most appropriate as an upscaled bulk horizontal permeability rather than adopting the highly localized 13,200 mD value of the thin uppermost layer. To constrain vertical flow within the reservoir, strong permeability anisotropy, expressed by the horizontal-to-vertical permeability ratio ($k_h/k_v = 100$), characterizes the formation and was thus imposed in the numerical model, which is consistent with values reported for petrophysically analogous carbonate geothermal systems [22]. This ratio was applied as a constant, homogeneous bulk property rather than a depth-dependent variable.

The available hydrochemical data show some variability in formation-water mineralization. Analyses from the Reus-1 well report two groups of salinity values, approximately 22–25 g/L and 31–32 g/L [28]. The original Reus-1 report describes the Jurassic formation waters as compositionally similar to those found in oil fields of the Gulf of Valencia and reports a total salinity of around 31 g/L, comparable to formation waters from the offshore Amposta-1 oil field. According to the Sulin classification, these Ca–Cl waters are classified as fossil, stagnant formation waters [31].

More recent formation-water analyses are available from the Reus-2 production tests [29]. The sum of the major dissolved constituents gives a TDS concentration of approximately 22.7 g/L for the upper test interval (1389–1430 m; electrical conductivity of 32,700 µS/cm) and 23.3 g/L for the broader tested interval (1389–1654 m; electrical conductivity of 33,400 µS/cm). Both samples therefore indicate a consistent formation-water

mineralization of approximately 23 g/L. It is important to note that while the regional model includes a halocline (density stratification transition zone) between 1000 and 1300 m depth, the targeted Jurassic reservoir is located at >2000 m depth, which is well below this transition. Therefore, the fluid within the target reservoir is characterized by a single stabilized salinity; therefore, the precise laboratory measurement of 22.676 g/kg was adopted to reflect the fluid conditions of the modeled area. This value was selected primarily from the Reus-2 data because these analyses are more recent, derive from documented production-test samples, and were obtained closer to the modeled target area. Characterizing such high-salinity brines within deep carbonate reservoirs is essential for understanding fluid-rock interactions in low-to-medium enthalpy geothermal systems, aligning with recent geochemical assessments of regional thermal aquifers in Mediterranean carbonate domains [32].

Regarding the regional structure, this implies the potential presence of normal faults between the shallower structural highs (where the Reus wells are located) and the deeper target area situated toward the northwest. Although the connectivity of faults in the subsurface and their detailed geometries are subject to regional uncertainty, the working geological hypothesis assumes the lateral continuity of the upper intervals of karstified dolomite. This highlights the value of the proposed workflow as a robust evaluation tool for decision-making during the early stages, which is characterized by a high degree of geological uncertainty.

3.6. Configuration for Reservoir and Techno-Economic Modeling and Parametric Sensitivity Analysis

The modeled area considered in the case study is shown by the red rectangle in Figure 5. The geothermal target is located in the subsurface immediately southwest of the Mas del Batlle industrial zone, west of the urban center of the city of Reus. The hypothetical production (red) and injection (blue) wells are designed to be directionally drilled from the industrial zone toward the southwest (SW) to reach the target reservoir.

The surface drilling platform is located at UTM coordinates X = 338,238 m, Y = 4,557,604 m (ETRS89, zone 31N). From this single surface location, the J-type directional wells are drilled toward the southwest. Geographically, the target area is situated at straight-line distances of approximately 3397 m from the historical Reus-3 well, 3673 m from Reus-2, and 4236 m from Reus-1.

Given the absence of deep boreholes directly within the target area and the associated spatial uncertainty, the geological, hydraulic, thermal, and hydrochemical properties derived from the Reus wells situated to the south were used as representative reservoir parameters in MRST for this case study. Constant-pressure boundary conditions were imposed along the model boundaries in the MRST simulations.

Due to urban constraints, a hypothetical energy consumption point is established at the Mas Batlle industrial park, designing a J-type directional doublet (Figure 6) to extract a base constant flow of 50 L/s with a single drilling pad close to the consumption area. The Kick-Off Point (KOP) was set at a depth of 1000 m. To prevent premature thermal short-circuiting, a minimum subsurface separation of at least 1000 m between targets was enforced. This geometric requirement yields an extreme Measured Depth (MD) of approximately 4800 m compared to a True Vertical Depth (TVD) of 2257 m (resulting in an MD/TVD ratio of 2.13). The production well considers (MD = 4803 m), and the injection well (MD = 4820 m).

Regarding the techno-economic analysis, the workflow natively estimates a baseline drilling capital cost based on the True Vertical Depth (TVD = 2257 m). To correctly account for the J-type well geometry, the actual monetary costs of the deviated trajectories are evaluated using their Measured Depths (MD_{PROD} = 4803 m and MD_{INJ} = 4820 m) in the polynomial cost correlation (Equation (4)). The ratio of this combined deviated drilling cost

to the vertical baseline cost yields a dimensionless adjustment multiplier of $f_{CAPEX} = 2.652$, which is then written directly into the GEOPHIRES-X input file.

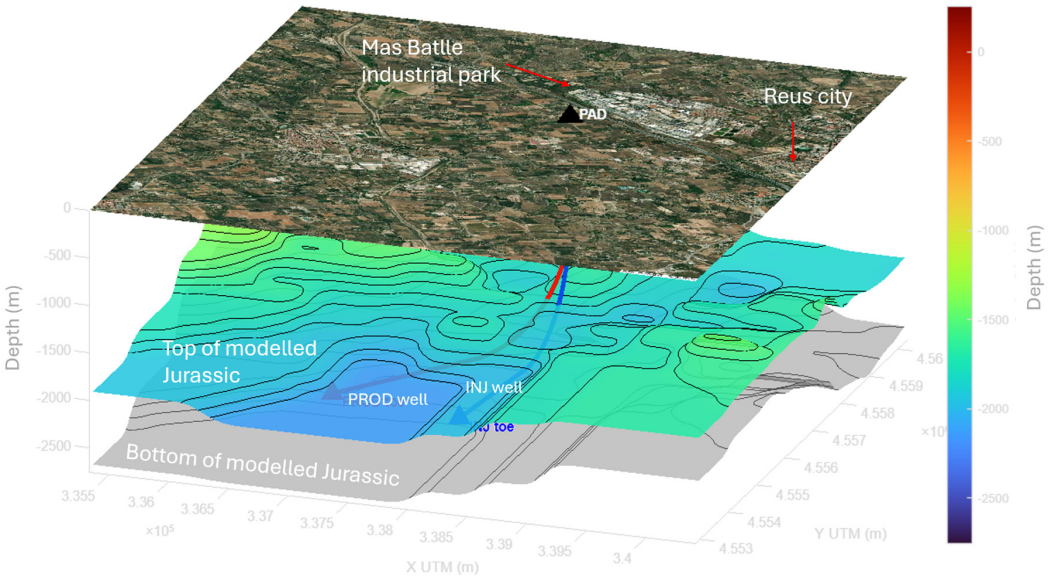

Figure 6. Three-dimensional view of the hypothetical geothermal doublet location considered in the MRST model, showing the deviated production and injection wells, together with the top and bottom surfaces of the Jurassic formation. The target reservoir considered in this case study corresponds to the uppermost 150 m of the Jurassic formation. The Jurassic top/bottom surfaces were extracted from the available regional-scale 3D geological–geothermal model [25].

The economic baseline considers a discount rate of 7%. This value was derived using the Weighted Average Cost of Capital (WACC) methodology, consistently aligned with the statutory rates of return established by the Spanish regulatory framework for renewable energies [33], supplemented by a 1% First-Of-A-Kind (FOAK) risk premium.

The plant utilization factor is set at 0.85 (approximately 7500 h/year), with a reinjection temperature of 50 °C. In this hypothetical scenario, a high-temperature, large-scale heat pump (HTHP) is integrated into the geothermal system to upgrade the available low-to-medium temperature geothermal fluid (70–90 °C) in the natural Jurassic reservoir to supply temperatures above 100 °C [34], thereby extending its potential use to high-temperature district heating and industrial processes. A very conservative seasonal Coefficient of performance (COP) of 2.5 was pre-fixed.

The OPEX includes a 2.5 times adjustment factor for wellfield maintenance to mitigate scaling risks associated with the high-salinity halocline.

Finally, a comprehensive risk assessment was automated using a One-Factor-at-a-Time (OFAT) sensitivity analysis over 11 parameters, applying uniform ±20% symmetrical variations. These 11 parameters were selected based on a combination of common techno-economic sensitivities reported in recent low-enthalpy geothermal literature and the specific geological uncertainties inherent to the ICGC 3D structural model. To improve computational efficiency, the Python orchestrator organizes the sensitivity runs into two execution levels: Level 1 for surface and macroeconomic variables (e.g., Discount Rate, Heat Sale Price, Electricity Rate), which freezes the physical simulation and iterates only GEOPHIRES-X, and Level 2 for geological and subsurface operational variables (e.g., Permeability, Production Flow Rate, Reinjection Temperature), which triggers the full MRST-GEOPHIRES-X coupled sequence. Furthermore, to ensure continuous execution during the OFAT sensitivity analysis, non-convergent numerical runs are managed via an exception-handling block

(try/catch). Any failed iterations are logged with null values (NaN) while the orchestrator automatically proceeds to the next parameter set without interrupting the batch process.

To ensure transparency and full reproducibility of the subsurface physical model, Table 2 summarizes all primary physical, operational and financial parameters implemented in the coupled MRST and GEOPHIRES-X architecture for the proof of concept. This table strictly defines the deterministic baseline scenario, and the associated parameter uncertainty ranges are systematically addressed via the sensitivity analysis in Section 4.3.

Table 2. Summary of baseline physical, operational, and financial parameters for the Camp Basin case study.

Parameter	Baseline Value	Source
Top Jurassic Permeability (upper 150 m) [mD]	2930	Reus-2 broader test interval [29], upscaled as bulk horizontal permeability.
Base Jurassic Permeability (>150 m) [mD]	1000	Conservative regional bulk assumption [25].
Permeability Anisotropy Ratio	100	Petrophysically analogous carbonate geothermal systems [22].
Reservoir Porosity	0.16	Regional geological model average [25].
Formation Brine Salinity (TDS) [g/kg]	22.67	Reus-2 fluid analysis [29].
Rock Density/Heat Capacity $\left[\mathrm{kg/m^3/J/(kg \cdot K)}\right]$	2630/1000	Standard regional carbonate properties [25].
Production Mass Flow Rate [kg/s]	50.8	Target operational constraint.
Reinjection Temperature [°C]	50	Target operational constraint.
Well Separation Distance [m]	1200	Geometric constraint for thermal short-circuit prevention.
True Vertical Depth (TVD) [km]	2.25	Derived from 3D Regional Geological Model.
Measured Depth (MD—Prod/Inj) [m]	4803/4820	Derived from 3D Regional Geological Model.
Well Completion Diameter [inch]	11.8	Standard API casing configuration.
Plant Lifetime [yrs]	30	Target operational constraint.
Plant Capacity/Utilization Factor (UF)	0.85	Standard techno-economic baseline (IRENA).
Discount Rate [%]	7	Regulatory Spanish WACC framework [33].
Heat Pump Coefficient of Performance (COP)	2.5	Conservative operational baseline
Well Drilling Cost Adjustment Factor (f_{CAPEX})	2.65	Calculated via Equation (4).

The simulation is discretized over a 30-year operational horizon divided into 128 adaptive time steps.

4. Results

4.1. Workflow Validation: Quantification of Analytical Bias

The primary validation of the developed workflow is based on quantifying the predictive divergence between a standalone analytical evaluation (using the internal models of GEOPHIRES-X for both physical and economic modeling) and the fully coupled numerical approach (MRST + GEOPHIRES-X). Both simulations were subjected to identical geometric, operational, and financial baseline parameters for the Camp Basin case study.

As detailed in Table 3, the comparison with the standalone analytical model illustrates how simplified reservoir representations may overestimate the techno-economic viability under the investigated conditions. By incorporating more realistic physical constraints, the coupled MRST–GEOPHIRES-X workflow reduces the net mean thermal power by 39.3% and the NPV by 91.2%, while increasing the LCOH by 71.9% relative to the standalone baseline.

Table 3. Comparison of techno-economic indicators between the standalone analytical model and the coupled numerical workflow for the base case scenario.

Indicator	Standalone Analytical	Coupled Workflow	Absolute Δ	Relative Δ
Net Present Value [MEUR]	36.19	3.18	−33.01	−91.2%
Internal Rate of Return [%]	15.88	9.01	−6.87 pp	-
LCOH [€/kWh$_{th}$]	0.0664	0.1141	+0.0477	+71.9%
Payback Period [Years]	8.08	11.95	+3.87	+47.9%
Net Mean Thermal Power [MWt]	12.77	7.75	−5.02	−39.3%
Total CAPEX [MEUR]	31.22	28.67	−2.55	−8.2%
Total OPEX [MEUR/year]	3.96	4.19	+0.23	+5.9%

The root cause of this divergence is the estimation of deliverable thermal power, where the standalone tool assumes a perfectly homogeneous and isotropic medium, calculating an idealized value of 12.77 MWt. In contrast, the coupled MRST simulation captures the actual non-homogeneous flow paths, vertical anisotropy, and salinity-induced buoyancy effects. Specifically, the vertical permeability anisotropy imposed in the proof-of-concept model ($K_h/K_v = 100$) significantly reduces vertical fluid migration and thermal convection. Furthermore, lithological stratification restricts fluid circulation, confining it primarily to high-permeability preferential pathways located within the first 150 m of the reservoir reducing the effective volumetric sweep efficiency compared to the ideal homogeneous radial displacement assumed in analytical models. These physical constraints restrict the actual extracted thermal power to 7.75 MWt (a 39.3% reduction). This massive reduction in thermal yield cascades through the economic module, drastically decreasing annual revenues and downgrading the project from highly profitable to only marginally viable. Regarding capital expenditures (CAPEX), it is important to note that the difference between the standalone analytical model (31.22 MEUR) and the coupled workflow (28.67 MEUR) is due to the sizing of the surface plant infrastructure. Since both scenarios incorporate the same adjustment factor for "J"-type directional drilling ($f_{\mathrm{CAPEX}} = 2.652$), the lower CAPEX in the coupled model directly reflects a smaller surface plant design, scaled proportionally to the lower thermal power supplied (7.75 MWt versus 12.77 MWt). Specifically, the 28.67 MEUR total CAPEX of the coupled model is fundamentally composed of drilling and completion costs (representing 71.5% of the total, approximately 20.50 MEUR) and the surface plant infrastructure, including ground facilities and the high-temperature heat pump (representing the remaining 28.5%, approximately 8.17 MEUR).

4.2. Thermo-Hydraulic Dynamics of the Coupled Model

The physical scope of the workflow was validated over a 30-year operational horizon. Despite the continuous extraction of 50 L/s, the J-type directional doublet demonstrates high thermal stability under the specific constant-pressure boundary conditions assumed for this proof of concept. The bottom-hole production temperature experiences a drop of $\Delta T = 0.35$ °C (from 75.62 °C to 75.27 °C) over the project's lifetime.

Regarding pressures, the highly transmissive carbonate formation establishes steady-state bottom-hole pressures of 225.5 bar at the producer and 229.1 bar at the injector, indicating excellent long-term injectivity facilitated by the high permeability of the target zone (2930 mD), which results in minimal parasitic pumping losses.

Assuming a natural reservoir temperature of 75 °C as a basis for energy calculations, and adopting an adjusted coefficient of performance (COP) of 2.5 together with a Carnot efficiency factor of 42%, as reported in previous studies [35], the resulting production temperature on the consumer side could reach approximately 145 °C. Large-scale and high-temperature heat pumps (HTHPs), as analyzed by [34], range widely in maturity depending on output temperature and design. Standard industrial heat pumps delivering up to 100–160 °C reach TRL 8 to 9 (market-available and proven in operation). The delivered supply temperature of approximately 145 °C therefore falls comfortably within the range of high-temperature heat pumps that are already commercially mature.

To provide a comprehensive understanding of the subsurface simulation behavior, the numerical results for a 30 year operational horizon are as follows. Bottom-hole pressures (BHP) remain stable at approximately 225.5 bar for the production well and 229.1 bar for the injection well, also with productivity and injectivity ($PI = 80.27$ kg/s·bar, $II = 56.29$ kg/s·bar). The gross thermal power extracted averages 9.25 MWt (resulting in a net usable thermal power of 7.75 MWt), with a negligible decrease in production temperature of only $\Delta T = 0.35$ °C (dropping from 75.62 °C to 75.27 °C).

The resulting spatial distribution of the thermal plume (Figure 7) confirms that the optimal 1200 m separation reached by the simulation effectively prevents the generation of a thermal short circuit. Finally, the plume remains confined within the upper 150 m of the Jurassic top, driven by permeability stratification and structural anisotropy. It should be noted that the absence of a massive, clearly defined cooling cone in the vicinity of the injection well is due to the visual threshold applied ($\Delta T > 1$ °C), in combination with the high transmissivity and advective heat-transport capacity of the karstified carbonate aquifer factors that rapidly disperse thermal anomalies horizontally, rather than creating a localized and stationary drop in temperature.

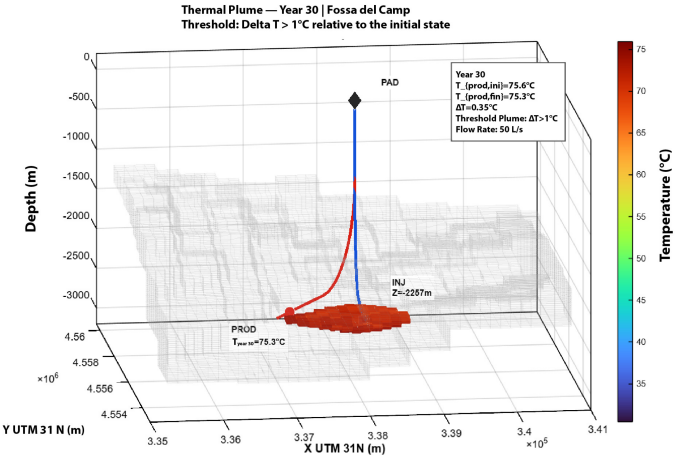

Figure 7. Spatial distribution of the 3D thermal plume within the Jurassic aquifer at year 30 ($\Delta T > 1$ °C).

4.3. Automated Parametric Sensitivity and Risk Hierarchy

Through the Python coupling interface, a One-Factor-at-a-Time (OFAT) sensitivity analysis loop was executed to generate risk profiles for the NPV and LCOH. The variables were subjected to uniform ±20% variations relative to the base case to ensure symmetric comparability (Figure 8). It is worth noting that this OFAT approach is implemented here as a straightforward deterministic test to illustrate the workflow's propagation of individual parameter perturbations rather than as an exhaustive probabilistic uncertainty assessment (e.g., Monte Carlo simulations).

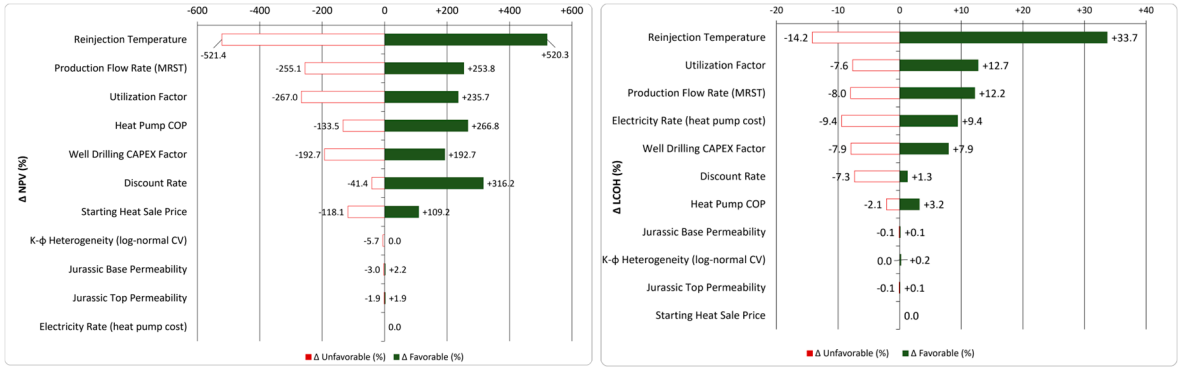

(**a**) (**b**)

Figure 8. Automated One-Factor-at-a-Time (OFAT) sensitivity analysis results. (**a**) Impact of parametric variations (±20%) on the Net Present Value (NPV). (**b**) Impact on the Levelized Cost of Heat (LCOH). It can be observed that geological parameters demonstrate minimal influence compared to operational and surface constraints.

Although heat pump electricity consumption constitutes a major component of OPEX, as reflected in a 9.4% variation in LCOH, a 20% change in the electricity tariffhas a negligible relative impact on NPV. This occurs because the NPV cash flow is heavily dominated by the initial CAPEX and gross thermal revenues, which mathematically overshadow the discounted fluctuations in electrical OPEX.

To provide absolute quantitative context to the risk hierarchy, Table 4 details the operational bounds of the most influential parameters under the ±20% variation scenario.

Table 4. Absolute bounds of NPV and LCOH under the ±20% sensitivity analysis.

Parameter	Min NPV (MEUR)	Max NPV (MEUR)	Min LCOH (€/kWh$_{th}$)	Max LCOH (€/kWh$_{th}$)
Reinjection Temperature	−13.40	19.80	0.098	0.153
Production Flow Rate	−4.93	11.25	0.105	0.128
Utilization Factor	−5.31	11.68	0.105	0.129
Heat Pump COP	−1.07	11.66	0.112	0.118
Discount Rate	2.17	15.40	0.106	0.124

The automated sensitivity analysis revealed a counterintuitive risk hierarchy for the targeted highly transmissive karstified Jurassic dolostone reservoir in the Camp Basin. Under the specific high transmissivity conditions investigated, reservoir parameters, such as permeability and spatial heterogeneity, showed a relatively limited influence on the project profitability, resulting in maximum NPV variations of less than 6%. This hierarchy of specific sensitivity is strictly constrained by the modeled baseline permeability of the reservoir and should not be generalized to sedimentary basins with lower permeability, where geological uncertainty could play a predominant role. Consequently, while the

inherent geological uncertainty of the subsurface remains high, the overall techno-economic performance of the project is relatively insensitive to variations in these properties within the explored parameter ranges.

Instead, the results indicate that financial risk is primarily controlled by surface thermodynamics, plant operations, and macroeconomic parameters. Reinjection temperature emerged as the technical variable with the greatest impact: reducing it from 50 °C to 40 °C maximizes heat extraction and raises the NPV to 19.8 MEUR, whereas increasing it to 60 °C limits thermal recovery and results in a negative NPV of −13.4 MEUR. Consequently, the coupled workflow suggests that for the highly transmissive reservoir conditions considered in this study, project optimization should primarily focus on maximizing useful heat extraction while carefully managing the potential geochemical risks associated with lower reinjection temperatures, particularly mineral precipitation and scaling resulting from temperature-induced changes in fluid–rock equilibrium. While reducing geological uncertainty through exploration remains fundamental for technical de-risking, these results highlight that optimizing surface thermodynamics and operational parameters is also critical for maximizing the financial viability of the project.

5. Discussion

The results of this study support the initial working hypothesis that techno-economic assessments based on simplified, uncoupled analytical reservoir models may introduce significant biases when applied to geologically complex geothermal systems. In the Camp Basin case study, the 3D MRST simulations captured reservoir-scale constraints associated with strong vertical anisotropy ($k_h/k_v = 100$) and the specific geometry of the J-type doublet, resulting in a 39.3% reduction in deliverable thermal power compared with the analytical representation. When these physically constrained thermal outputs were incorporated into GEOPHIRES-X, the estimated project profitability decreased accordingly.

In its standalone configuration, GEOPHIRES-X relies on simplified analytical reservoir representations based on idealized and homogeneous conditions. More detailed reservoir behavior can be incorporated through coupling with numerical reservoir simulators such as the license-based TOUGH2, as demonstrated in previous studies. While simplified analytical approaches remain appropriate for preliminary assessments, the results of this case study indicate that their application to geologically and structurally complex 3D reservoir settings may lead to overly optimistic estimates of project profitability and, consequently, financial viability. The loose-coupling strategy developed here provides an open-component coupling alternative by linking MRST and GEOPHIRES-X through a Python-based interface, enabling the automated transfer of reservoir simulation outputs to the techno-economic model and facilitating systematic sensitivity analyses without manual data transcription.

The OFAT sensitivity analysis identified reinjection temperature as the operational parameter exerting the strongest influence on project economics within the investigated ranges. Reducing the reinjection temperature from 50 °C to 40 °C increases useful heat extraction and improves NPV. However, this apparent economic benefit must be considered alongside potential operational and geochemical constraints. In highly saline geothermal fluids (>22 g/kg TDS), lower reinjection temperatures may alter fluid–mineral equilibria and potentially promote $CaCO_3$ precipitation and scaling, with associated implications for chemical treatment, wellfield maintenance, and OPEX. Since these geochemical processes were not explicitly modeled in the present workflow, the economically optimal reinjection temperature should not necessarily be interpreted as the technically optimal operating condition. While lowering the reinjection temperature to 40 °C enhances the project's economic performance, this benefit must be balanced against potential operational limitations such as increased mineral scaling, precipitation risks, injectivity decline, and thermal stress.

The thermal stability observed over the 30-year simulation horizon ($\Delta T = 0.35$ °C) should also be interpreted in the context of the adopted numerical setup. Constant-pressure boundary conditions and the lateral truncation of the regional Camp Basin geological grid, implemented to reduce computational load and memory requirements, may contribute to the relatively limited thermal decline observed during the simulation period. Although this configuration is adequate for demonstrating the coupled workflow, future site-specific assessments should investigate long-term thermal drawdown using alternative boundary conditions, including closed or semi-closed configurations, and larger-scale basin geometries.

The sensitivity analysis itself also presents methodological limitations. The One-Factor-at-a-Time (OFAT) approach is computationally efficient and useful for identifying first-order sensitivities, but it does not capture non-linear interactions or correlations among parameters. A logical extension of the workflow would therefore be the implementation of stochastic approaches, such as Monte Carlo simulations, in which probability distributions are assigned to uncertain input parameters to derive probabilistic estimates of NPV and LCOH (e.g., P10, P50, and P90). Furthermore, the relatively limited influence of geological parameters on NPV observed in this study should not be interpreted as reduced geological uncertainty. Rather, it reflects the exceptionally high transmissivity of the targeted karstified Jurassic dolostone reservoir within the parameter ranges investigated. Application of the workflow to tighter, matrix-dominated sedimentary reservoirs could reveal substantially different geological, operational, and economic sensitivity hierarchies.

From a broader energy-transition perspective, the proposed architecture provides an auditable, reproducible, automated, and open-component coupling framework for integrating 3D reservoir physics into geothermal techno-economic assessment. Its Python-based coupling interface enables systematic screening and comparison of multiple development scenarios while retaining the physical constraints represented by numerical reservoir simulations and avoiding dependence on proprietary reservoir simulation software. This capability may be particularly valuable for early-stage assessment and investment decision-making for geothermal resources targeting district heating and industrial heat decarbonization.

6. Conclusions

This study developed and demonstrated an automated, open-component computational workflow that couples the 3D thermo-hydraulic reservoir simulation capabilities of MRST with the techno-economic evaluation framework of GEOPHIRES-X. The workflow enables physically constrained simulated reservoir outputs to be directly incorporated into techno-economic assessments, bypassing the simplified analytical reservoir representation used in the standalone configuration.

Finally, it is important to note that this study serves primarily as a methodological demonstration of the open-component coupling framework. The specific physical and economic results obtained, such as thermal stability ($\Delta T = 0.35$ °C) and low sensitivity to geological parameters, are characteristic of the constant boundary conditions and natural transmissivity imposed for the Camp basin. Consequently, the numerical results obtained should not be directly extrapolated to other geological settings, such as reservoirs with a low-permeability matrix, systems with closed or semi-closed boundaries, , or scenarios without constraints imposed by existing wells, since these conditions would require different modeling assumptions and stimulation strategies

Prioritizing methodological integration over site-specific prospecting, the application of the workflow to a hypothetical J-type geothermal doublet targeting the karstified Jurassic dolostone reservoir in the Camp Basin led to three main conclusions:

- **Impact of reservoir representation on project economics**: The standalone analytical approach overestimated the NPV by 91.2% and underestimated the LCOH by 71.9%

compared with the fully coupled MRST-GEOPHIRES-X simulation (as detailed in Table 3), demonstrating that reservoir representation can materially affect estimates of the project viability.

- **Importance of 3D physical constraints:** The 3D reservoir simulation captured the effects of the J-type well geometry and strong vertical anisotropy ($K_h/K_v = 100$) on thermal plume development, resulting in a 39.3% reduction in deliverable thermal power (Table 3), relative to isotropic analytical assumptions. Moreover, the thermal stability observed over a 30-year period remains intrinsically linked to the open boundary conditions applied in this methodological demonstration, which highlights that for future site-specific developments, it is essential to rigorously evaluate regional boundary limits.
- **Shift in techno-economic sensitivity**: Under the highly transmissive reservoir conditions investigated, uncertainties in subsurface geological parameters such as permeability had a relatively limited influence on project economics within the ranges investigated, a specific condition of the high permeability regime in this proof of concept rather than a universal rule. Instead, the sensitivity analysis identified operational parameters, particularly reinjection temperature, as dominant controls on economic performance (Figure 8).

Overall, the proposed MRST-GEOPHIRES-X workflow provides a reproducible and open-component coupling framework for evaluating how 3D subsurface physical constraints propagate into geothermal project economics and for systematically exploring alternative development scenarios. The results highlight the value of incorporating detailed reservoir physics into techno-economic assessments, particularly when evaluating geologically complex geothermal systems at the local or prospect scale, specifically within low-to-medium enthalpy regimes oriented toward direct heat use and industrial decarbonization.

Author Contributions: Conceptualization, D.V.L. and I.H.; methodology, D.V.L. and I.H.; software, D.V.L.; validation, I.H. and E.G.-R.; formal analysis, D.V.L.; investigation, D.V.L.; resources, I.H.; data curation, D.V.L.; writing—original draft preparation, D.V.L.; writing—review and editing, I.H. and E.G.-R.; visualization, D.V.L.; supervision, I.H. and E.G.-R.; project administration, I.H.; funding acquisition, I.H. All authors have read and agreed to the published version of the manuscript.

Funding: This research was funded by the Institut Cartogràfic i Geològic de Catalunya (ICGC) through a student grant awarded to the first author, D.V., within the Master's Degree in Renewable Energy and Energy Sustainability, Faculty of Physics, University of Barcelona (UB), 08028 Barcelona, Spain.

Data Availability Statement: The original contributions presented in this study are included in the article. Further inquiries can be directed to the corresponding authors.

Acknowledgments: During the preparation of this manuscript, the author(s) used Gemini (versions 3.1 Pro and 3.6 Flash) and Claude (Sonnet 5) for the purposes of text translation, paragraph restructuring, and improving overall section organization and readability. The authors have reviewed and edited the output and take full responsibility for the content of this publication.

Conflicts of Interest: The authors declare no conflicts of interest.

Abbreviations

The following abbreviations are used in this manuscript:

BHP	Bottom-Hole Pressure
CAPEX	Capital Expenditure
COP	Coefficient of Performance
ICGC	Institut Cartogràfic i Geològic de Catalunya

LCOH	Levelized Cost of Heat
HTHP	High-Temperature Heat Pump
MD	Measured Depth
MRST	MATLAB Reservoir Simulation Toolbox
NPV	Net Present Value
OFAT	One-Factor-at-a-Time
OPEX	Operational Expenditure
TVD	True Vertical Depth
WACC	Weighted Average Cost of Capital

References

1. Lowell, R.; Gringarten, A. Comments on "Theory of Heat Extraction from Fractured Hot Dry Rock" by A. C. Gringarten et al. *J. Geophys. Res.* **1976**, *81*, 359–360. [CrossRef]
2. Lie, K.-A. *An Introduction to Reservoir Simulation Using MATLAB/GNU Octave: User Guide for the MATLAB Reservoir Simulation Toolbox (MRST)*; Cambridge University Press: Cambridge, UK, 2019.
3. Collignon, M.; Klemetsdal, Ø.S.; Møyner, O.; Alcanié, M.; Rinaldi, A.P.; Nilsen, H.; Lupi, M. Evaluating Thermal Losses and Storage Capacity in High-Temperature Aquifer Thermal Energy Storage (HT-ATES) Systems with Well Operating Limits: Insights from a Study-Case in the Greater Geneva Basin, Switzerland. *Geothermics* **2020**, *85*, 101773. [CrossRef]
4. Khedekar, V.V.; Memon, A.R.A.N.; Pal, M. Efficient Geothermal Reservoir Simulation Using Deep Learning Surrogates and Multiscale Interpolation Techniques. *Processes* **2026**, *14*, 1248. [CrossRef]
5. Beckers, K.F.; McCabe, K. GEOPHIRES v2.0: Updated Geothermal Techno-Economic Simulation Tool. *Geotherm. Energy* **2019**, *7*, 5. [CrossRef]
6. European Geothermal Energy Council (EGEC). *EGEC Geothermal Market Report 2024: Key Findings*; EGEC: Brussels, Belgium, 2024.
7. Pruess, K.; Oldenburg, C.; Moridis, G. *TOUGH2 User's Guide, Version 2.0*; Lawrence Berkeley National Laboratory: Berkeley, CA, USA, 1999.
8. Memon, A.R.; Makauskas, P. Modeling Thermal Front Dynamics in Geothermal Reservoirs Using an Open-Source MRST-MATLAB Simulation Framework. *Adv. Carbon Capture Util. Storage* **2026**, *4*, 55–60. [CrossRef]
9. Nan, T.; Hu, T.; Wang, Z.; Zhang, J.; Yin, J.; Xie, Y.; Wu, J.; Lu, C. Modeling Hydro-Thermal Processes in Fractured Geothermal Reservoirs Using Embedded Discrete Fracture Model (EDFM) and MRST. *Adv. Water Resour.* **2025**, *206*, 105120. [CrossRef]
10. Shi, D.; Cheng, S.; Wang, Q.; Liu, D.; Yin, F.; Xu, X.; Guo, X.; Weng, Z. Comparative Analysis and Application of Mass and Heat Transfer Simulation in Fractured Reservoirs Based on Two Fracture Models. *Processes* **2024**, *12*, 2399. [CrossRef]
11. Li, X.; Xue, Y.; Dang, F.; Ranjith, P.G.; Xie, H.; Hou, P.; Cai, C. Microscale Damage Evolution of High-Temperature Granite under Liquid Nitrogen Thermal Shock Based on Computed Tomography Analysis. *Eng. Geol.* **2025**, *356*, 108274. [CrossRef]
12. Xue, Y.; Li, X.; Wang, L.; Liu, Y.; Cao, X.; Zhang, Y. Mesoscopic Damage Enhancement in Granite under Cyclic Liquid Nitrogen Shocks Characterized by Computed Tomography and Texture Analysis. *Int. J. Rock Mech. Min. Sci.* **2025**, *194*, 106217. [CrossRef]
13. Pokhrel, A.; Hoyos, L.R.; Yu, X. Modeling Thermal Conductivity of Sandy Soils Under Unfrozen Temperature Conditions. *Geosciences* **2026**, *16*, 175. [CrossRef]
14. Aghaei, H.; Colombera, L.; Yan, N.; Mountney, N.P.; Andersen, O.; Di Giulio, A. Capturing Scales of Heterogeneity in Models of Fluvial Geothermal Reservoirs: Grid Resolution, Upscaling Strategies, and Hierarchies of Sedimentary Architecture. *Adv. Water Resour.* **2026**, *209*, 105217. [CrossRef]
15. Jia, P.; Guo, H.; Gao, H. Studying the Impact of Pore Sizes on Gas Flow and Distribution in Volatile Carbonate Reservoirs Using a New Triple-Porosity Model. *Phys. Fluids* **2024**, *36*, 103103. [CrossRef]
16. Gao, M.; Sun, W.; Xu, J.; Li, J. Reduced-Order Modeling for Subsurface Flow Simulation in Fractured Reservoirs. *SPE J.* **2025**, *30*, 391–408. [CrossRef]
17. National Laboratory of the Rockies. GEOPHIRES-X: Open-Source Geothermal Techno-Economic Simulator. 2026. Available online: https://github.com/NREL/GEOPHIRES-X (accessed on 18 August 2026).
18. Jung, Y.; Pau, G.S.H.; Finsterle, S.; Doughty, C. *TOUGH3 User's Guide, Version 1.0*; Lawrence Berkeley National Laboratory: Berkeley, CA, USA, 2018.
19. Liu, X.; Geng, S.; Sun, J.; Li, Y.; Guo, Q.; Zhan, Q. Novel Coupled Hydromechanical Model Considering Multiple Flow Mechanisms for Simulating Underground Hydrogen Storage in Depleted Low-Permeability Gas Reservoir. *Int. J. Hydrog. Energy* **2024**, *85*, 526–538. [CrossRef]
20. Cardona, A.; Finkbeiner, T.; Santamarina, J.C. Hydro-Mechanical Coupling in Fractured Rocks: A Numerical Study Using the Implicit Joint-Continuum Model. *Int. J. Rock Mech. Min. Sci.* **2026**, *200*, 106460. [CrossRef]
21. Liao, X.; Zhou, J.; Wang, P.; Liu, F.; Shang, X. Coupling of Peridynamics and MRST for Simulation of Hydraulic Fracturing in Porous Media. *Comput. Geotech.* **2026**, *191*, 107760. [CrossRef]

22. Antwi, K.; Amber, I.; Oluyemi, G. A Coupled Numerical Model to Assess the Caprock Geochemical Integrity and Porosity Change of an Underground Hydrogen Gas Storage System. *Int. J. Hydrog. Energy* **2025**, *109*, 624–635. [CrossRef]
23. Bertoni, L.; Møyner, O.; Wiegner, J.; Gazzani, M. Optimizing Carbon Capture and Storage Infrastructure Including Physics-Based Reservoir Modelling. *Comput. Chem. Eng.* **2025**, *202*, 109293. [CrossRef]
24. Collignon, M.; Klemetsdal, Ø.S.; Møyner, O. Simulation of Geothermal Systems Using MRST. In *Advanced Modelling with the MATLAB Reservoir Simulation Toolbox*; Lie, K.-A., Møyner, O., Eds.; Cambridge University Press: Cambridge, UK, 2021; pp. 491–514.
25. Institut Cartogràfic i Geològic de Catalunya (ICGC). *Deep Geothermal Resource Assessment in the Mesozoic Reservoirs of the Camp Basin*; ICGC: Barcelona, Spain, 2023. Available online: https://datacloud.icgc.cat/datacloud/descarregues-web/bd/pubs/icgc_TR_0001_23_en.pdf (accessed on 19 August 2026).
26. Saad, Y.; Schultz, M.H. GMRES: A Generalized Minimal Residual Algorithm for Solving Nonsymmetric Linear Systems. *SIAM J. Sci. Stat. Comput.* **1986**, *7*, 856–869. [CrossRef]
27. European Central Bank (ECB). *Euro Foreign Exchange Reference Rates: US Dollar (USD)*; Monthly Average; European Central Bank (ECB): Frankfurt am Main, Germany, 2026.
28. Echánove, I.; Núñez, A.; Piérard, H. *Informe Geológico Final Del Sondeo Reus-1*; American Petrofina Exploration Company, Sucursal Española: Madrid, Spain, 1976.
29. Enagás. *Informe Geológico Del Sondeo Reus-2*; Enagás: Madrid, Spain, 1999.
30. Enagás. *Informe Geológico Del Sondeo Reus-3*; Enagás: Madrid, Spain, 2001.
31. Enagás-Aurensa. *Proyecto de Almacenamientos Subterráneos de Gas: Reus*; Enagás: Madrid, Spain, 1996.
32. Cangemi, M.; Oliveri, Y.; Inguaggiato, S.; Favara, R.; Madonia, P. Geochemical Behavior of Rare Earth Elements in Hydrothermal Groundwaters of Western Sicily (Italy). *Geosciences* **2026**, *16*, 379. [CrossRef]
33. Gobierno de España. Real Decreto-Ley 17/2019, de 22 de Noviembre, Por El Que Se Adoptan Medidas Urgentes Para La Adaptación de Parámetros Retributivos Que Afectan al Sistema Eléctrico. In *Boletín Oficial del Estado*; Gobierno de España: Madrid, Spain, 2019; pp. 128615–128646.
34. Elwardany, M.; Turja, A.I.; Hasan, M.M.; Nassif, N. High-Temperature Heat Pumps for Industrial Decarbonization: Technologies, Integration Strategies, and Future Perspectives. *Chem. Eng. Process.-Process Intensif.* **2026**, *225*, 110806. [CrossRef]
35. Gustafson, J.O.; Smith, J.D.; Beyers, S.M.; Al Aswad, J.A.; Jordan, T.E.; Tester, J.W. Earth Source Heat: Feasibility of Deep Direct-Use of Geothermal Energy on the Cornell Campus. *GRC Trans.* **2018**, *42*, 1379–1394.

Disclaimer/Publisher's Note: The statements, opinions and data contained in all publications are solely those of the individual author(s) and contributor(s) and not of MDPI and/or the editor(s). MDPI and/or the editor(s) disclaim responsibility for any injury to people or property resulting from any ideas, methods, instructions or products referred to in the content.